# Effects of Zero-Point Energy Difference on Intramolecular Electron Transfer in Asymmetric Polyethyl-Substituted Biferrocenium Triiodides

**Teng-Yuan Dong,*[1a] Po-Ju Lin,[1a] and Kuan-Jiuh Lin[1b]**

Department of Chemistry, National Sun Yat-sen University, Kaohsiung, Taiwan 804, ROC, and The Institute of Chemistry, Academia Sinica, Nankang, Taipei, Taiwan, ROC

*Received July 28, 1995*[⊗]

The syntheses, characterizations, and physical properties of asymmetric polyethyl-substituted mixed-valence 1′,2′,1‴-triethylbiferrocenium triiodide (**15**), 1′,3′,1‴-triethylbiferrocenium triiodide (**16**), and 1′,2′,1‴,3‴-tetraethylbiferrocenium triiodide (**17**) are described. Complexes **15**−**17** were characterized by electrochemical measurements and by near-IR, $^{57}$Fe Mössbauer, and paramagnetic $^{1}$H NMR spectroscopy. These complexes are found to be localized on the $^{57}$Fe Mössbauer time scale (electron-transfer rates less than $10^7$ s$^{-1}$). The cations in complexes **15**−**17** are not in equivalent environments. This asymmetry results in a nonzero zero-point energy barrier for intramolecular electron transfer. Analysis of the sign of contact shifts suggests that the electron delocalization in **15**−**17** is based on competing $\sigma$ and $\pi$ delocalization mechanisms. The X-ray structure of **15** has been determined at 298 K: monoclinic, $P2_1/n$, $a$ = 9.962(3) Å, $b$ = 20.610(3) Å, $c$ = 13.326(3) Å, $\beta$ = 92.74(2)°, $Z$ = 4, $D_{calcd}$ = 2.029 g cm$^{-3}$, $R_F$ = 0.033, $R_{wF}$ = 0.036. The neutral compound 1′,2′,1‴-triethylbiferrocene crystallizes in the triclinic space group $P\bar{1}$ with two molecules in a unit cell with dimensions $a$ = 7.465(3), $b$ = 8.419(2), $c$ = 18.581(4) Å and $\alpha$ = 87.83(2), $\beta$ = 87.98(3), $\gamma$ = 64.27(2)°; $R_F$ = 0.021 and $R_{wF}$ = 0.029.

## Introduction

Over the last decade, electron transfer (ET) processes in both solid and solution states have been among the most important subjects in chemistry and biology.[2] Recently, we reported systematic studies for ET in the solid state for a series of mixed-valence biferrocenium cations (**1**−**8**), which have led to a wealth of new experimental results.[3−12] Major progress has been made in studying the dependence of ET rates on the lattice dynamics[3−6] and on the cation−anion interactions,[13−15] as well as on the structural micromodification.[7] More recently, we prepared a series of polyalkylbiferrocenium triiodide salts (**9**−**14**) to study the influence of ring tilt between two least-squares-fitted cyclopentadienyl (Cp) rings on ET and to investigate energetic control of ET rates.[16−18] Deviations of the Cp rings from the parallel position were found to correlate quite well with the critical temperature for electronic delocalization−localization in mixed-valence biferrocenium salts.

However, despite these extensive studies, there has, in fact, been little reported concerning the ET in asymmetric biferrocenium triiodide in the solid state.[10] The present work will focus on the spectroscopic measurements for mixed-valence cations (**15**−**17**). The understanding of electron-transfer processes in **15**−**17** provides detailed insight into the fundamental theoretical aspect of the zero-point energy difference.[19,20] The effect of the zero-point energy difference on the ET rate will be discussed. Thus the general importance of this study is that it is a test case for the most fundamental concepts of ET processes in the solid state. The results of the X-ray structural work on **15** together with the variable-temperature $^{57}$Fe Mössbauer data, electrochemical measurements, and IR data are presented in this paper.

## Experimental Section

**General Information.** All manipulations involving air-sensitive materials were carried out by using standard Schlenk techniques under

⊗ Abstract published in *Advance ACS Abstracts*, September 1, 1996.

(1) (a) National Sun Yat-sen University. (b) Academia Sinica.
(2) (a) Holm, R. H. In *Biological Aspects of Inorganic Chemistry*; Addison, A. W., Cullen, W. R., Dolphin, D., James, B. R., Ed.; Wiley: New York, 1977; Chapter 2. Nherland, S.; Gray, H. B. *Ibid*., Chapter 10. (b) Lacoste, M.; Rabaa, H.; Astruc, D.; Ardoin, N.; Varret, F.; Saillard, J.-Y.; Beaze, A. L. *J. Am. Chem. Soc*. **1990**, *112*, 9548 and references therein. (c) Day, P. *Int. Rev. Phys. Chem*. **1981**, *1*, 149. (d) Brown, D. B., Ed. *Mixed-Valence Compounds, Theory and Applications in Chemistry, Physics, Geology, and Biology*; Reidel: Boston, MA, 1980. (e) Creutz, C. *Prog. Inorg. Chem*. **1983**, *30*, 1. (f) Richardson, D. E.; Taube, H. *Coord. Chem. Rev*. **1984**, *60*, 107. (g) Hendrickson, D. N.; Oh, S. M.; Dong, T.-Y.; Moore, M. F. *Comments Inorg. Chem*. **1985**, *4*, 329.
(3) (a) Cohn, M. J.; Dong, T.-Y.; Hendrickson, D. N.; Geib, S. J.; Rheingold, A. L. *J. Chem. Soc., Chem. Commun*. **1985**, 1095. (b) Dong, T.-Y.; Hendrickson, D. N.; Iwai, K.; Cohn, M. J.; Rheingold, A. L.; Sano, H.; Motoyama, I.; Nakashima, S. *J. Am. Chem. Soc*. **1985**, *107*, 7996.
(4) Iijima, S.; Saida, R.; Motoyama, I.; Sano, H. *Bull. Chem. Soc. Jpn*. **1981**, *54*, 1375.
(5) Nakashima, S.; Katada, M.; Motoyama, I.; Sano, H. *Bull. Chem. Soc. Jpn*. **1987**, *60*, 2253.
(6) Kai, M.; Katada, M.; Sano, H. *Chem. Lett*. **1988**, 1523.
(7) Dong, T.-Y.; Lee, T.-Y.; Lee, S. H.; Lee, G. H.; Peng, S. M. *Organometallics* **1994**, *13*, 2337.
(8) Dong, T.-Y.; Ke, T. J.; Peng, S. M.; Yeh, S. K. *Inorg. Chem*. **1989**, *28*, 2103.
(9) Dong, T.-Y.; Hwang, M. Y.; Wen, Y. S. *J. Organomet. Chem*. **1990**, *391*, 377.
(10) Dong, T.-Y.; Schei, C. C.; Hsu, T. L.; Lee, S. L.; Li, S. J. *Inorg. Chem*. **1991**, *30*, 2457.
(11) Webb, R. J.; Geib, S. J.; Staley, D. L.; Rheingold, A. L.; Hendrickson, D. N. *J. Am. Chem. Soc*. **1990**, *112*, 5031.
(12) Dong, T.-Y.; Kambara, T.; Hendrickson, D. N. *J. Am. Chem. Soc*. **1986**, *108*, 5857.
(13) Kambara, T.; Hendrickson, D. N.; Dong, T.-Y.; Cohn, M. J. *J. Chem. Phys*. **1987**, *86*, 2362.
(14) Dong, T.-Y.; Huang, C. H.; Chang, C. K.; Hsieh, H. C.; Peng, S. M.; Lee, G. H. *Organometallics* **1995**, *14*, 1776.
(15) Dong, T.-Y.; Schei, C. C.; Hwang, M. Y.; Lee, T. Y.; Yeh, S. K.; Wen, Y. S. *Organometallics* **1992**, *11*, 573.
(16) Dong, T.-Y.; Chang, C. K.; Huang, C. H.; Wen, Y. S.; Lee, S. L.; Chen, J. A.; Yeh, W. Y.; Yeh, A. *J. Chem. Soc., Chem. Commun*. **1992**, 526.
(17) Dong, T.-Y.; Huang, C. H.; Chang, C. K.; Wen, Y. S.; Lee, S. L.; Chen, J. A.; Yeh, W. Y.; Yeh, A. *J. Am. Chem. Soc*. **1993**, *115*, 6357.
(18) Dong, T.-Y.; Lee, S. H.; Chang, C. K. Unpublished results.
(19) Wong, K. Y.; Schatz, P. N. *Prog. Inorg. Chem*. **1981**, *28*, 369.
(20) Hush, N. S. *Prog. Inorg. Chem*. **1967**, *8*, 391.

S0020-1669(95)00953-0 CCC: $12.00 

**Chart 1**

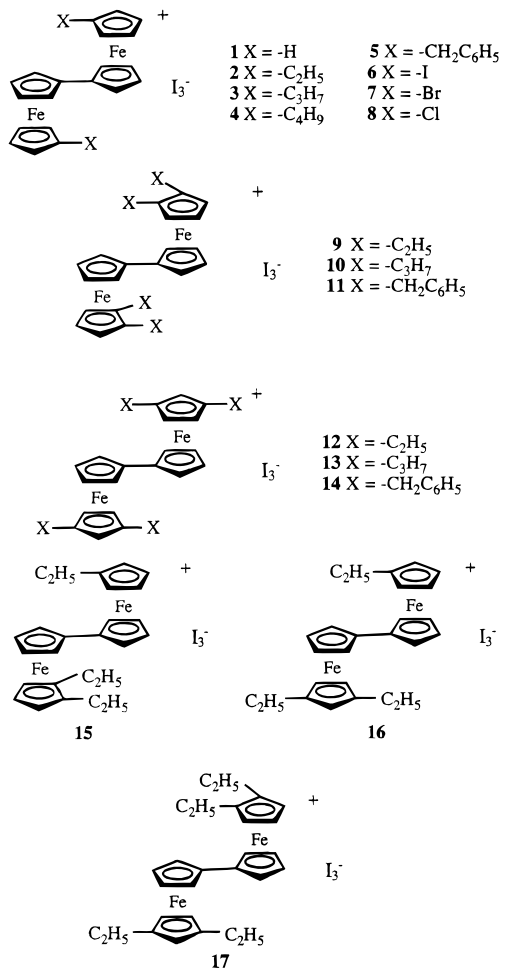


an atmosphere of nitrogen (Scheme 1). Chromatography was performed on neutral alumina (activity II), eluting with hexane/$CH_2Cl_2$. Dichloromethane was dried over $P_2O_5$. Samples of 1′-acetyl-2′-ethyl-1-bromoferrocene (**19**), 1′-acetyl-3′-ethyl-1-bromoferrocene (**25**), 1′,3′-diethyl-1-bromoferrocene (**22**), and 1′-acetyl-1-bromoferrocene (**18**) were prepared according to the literature procedure[17] and identified by melting point and NMR and mass spectra.

**Ullmann Coupling of 18 and 19.** A mixture of the corresponding bromoferrocenes (**18** (1.13 g, 3.68 mmol) and **19** (1.18 g, 3.52 mmol)) and activated copper (5 g) was heated under $N_2$ at 110−120 °C for 24 h. After cooling to room temperature, the reaction mixture was repeatedly extracted with $CH_2Cl_2$ until the extracts appeared colorless. The extracts were evaporated and chromatographed. The first and second bands eluting with hexane/ethyl acetate (50:1) were the starting materials **19** and **18**, respectively. The third band eluting with hexane/ethyl acetate (25:1) was 1′,1‴-diacetyl-2′,2‴-diethylbiferrocene (0.3 g, 16.7% yield). The fourth band eluting with hexane/ethyl acetate (15:1) was **20** (0.39 g, 23% yield). The last band eluting with hexane/ethyl acetate (10:1) was the known compound 1′,1‴-diacetylbiferrocene (0.2 g, 13% yield) characterized by $^1$H NMR. Compounds of 1′,1‴-diacetyl-2′,2‴-diethylbiferrocene and **20** were recrystallized from benzene/hexane. The physical properties of 1′,1‴-diacetyl-2′,2‴-diethylbiferrocene are as follows. $^1$H NMR ($CDCl_3$, ppm): 1.04 (t, 6H, $-CH_3$), 2.16 (s, 6H, $-COCH_3$), 2.38 (m, 2H, $-CH-$), 2.62 (m, 2H, $-CH-$), 4.16 (t, 2H, Cp), 4.20 (m, 6H, Cp), 4.24 (t, 2H, Cp), 4.26 (t, 2H, Cp), 4.40 (q, 2H, Cp). Mass spectrum: $M^+$ at *m*/*z* 510. Mp: 84−86 °C. The physical properties of **20** are as follows. $^1$H NMR ($CDCl_3$, ppm): 1.04 (t, 3H, $-CH_3$), 2.13 (s, 3H, $-COCH_3$), 2.17 (s, 3H, $-COCH_3$), 2.40 (m, 1H, $-CH-$), 2.62 (m, 1H, $-CH-$), 4.16 (t, 1H, Cp), 4.20 (s, 4H, Cp), 4.26 (m, 4H, Cp), 4.30 (t, 2H, Cp), 4.36 (m, 1H, Cp), 4.40 (m, 1H, Cp), 4.56 (t, 2H, Cp). Mass spectrum: $M^+$ at *m*/*z* 482. Mp: 128.1−129 °C.

**Ullmann Coupling of 18 and 22.** The coupling reaction of **18** (1.78 g, 5.54 mmol) and **22** (1.70 g, 5.54 mmol) was carried out according to the same procedure as the coupling of **18** and **19**. The red oily residue was chromatographed on alumina. The first band eluting with hexane was the recovered starting material (**22**, 0.6 g). Continued elution with hexane produced 1′,3′,1‴,3‴-tetraethylbiferrocene (0.5 g, 2% yield). Continued elution with hexane/ethyl acetate (50:1) gave acetylferrocene (third band, 0.24 g, 17.9% yield), 1′-acetyl-1-bromoferrocene (fourth band, 0.06 g, 3.5% yield), and the desired compound **23** (fifth band, 0.05 g, 2% yield). The last band eluting with hexane/ethyl acetate (15:1) was 1′,1‴-diacetylbiferrocene (0.95 g, 38% yield). All compounds were identified with $^1$H NMR and mass spectra. The physical properties of the new compound **23** are as follows. $^1$H NMR ($CDCl_3$, ppm): 1.03 (t, 6H, $-CH_3$), 2.09 (q, 4H, $-CH_2-$), 2.14 (s, 3H, $-COCH_3$), 3.74 (s, 3H, Cp), 4.12 (t, 2H, Cp), 4.18 (t, 2H, Cp), 4.21 (t, 2H, Cp), 4.31 (t, 2H, Cp), 4.36 (t, 2H, Cp), 4.56 (t, 2H, Cp). Mass spectrum: $M^+$ at *m*/*z* 468. Mp: 71.5−72.4 °C.

**Scheme 1.** Reagents and Conditions: (i) Activated Cu; (ii) $AlCl_3/LiAlH_4$; (iii) $I_2$

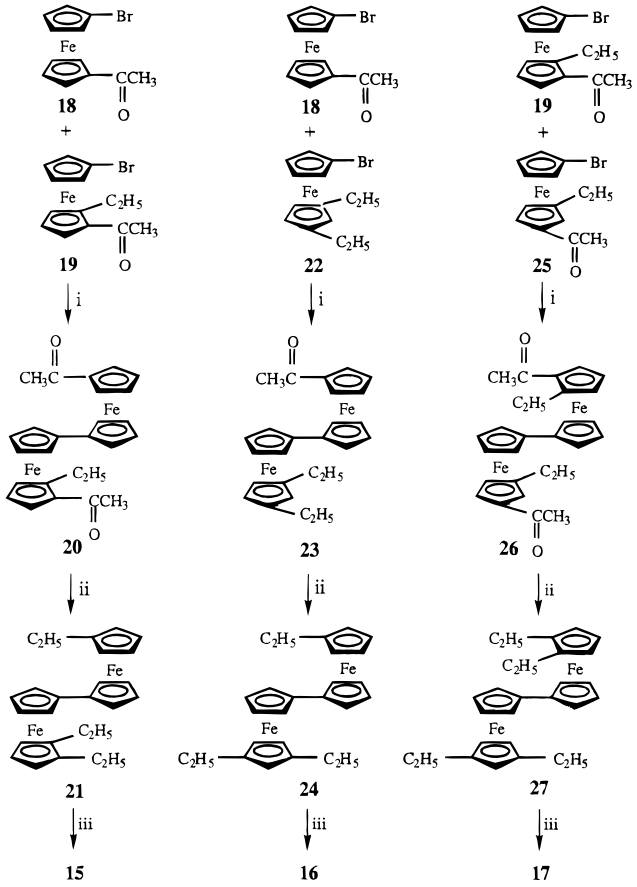


**Ullman Coupling of 19 and 25.** The coupling reaction of **19** and **25** was carried out in a manner similar to the procedure for coupling of **18** and **19**. After evaporation of the solvent, the mixture was chromatographed on $Al_2O_3$. The first and second bands were 1-acetyl-2-ethylferrocene (0.22 g, 31%) and 1-acetyl-3-ethylferrocene (0.20 g, 28%) eluting with hexane/ethyl acetate (50:1). The third band eluting with hexane/ethyl acetate (15:1) was 1′,1‴-diacetyl-2′,2‴-diethylbiferrocene (0.17 g, 12%). The fourth band eluting with hexane/ethyl acetate (10:1) was 1′,1‴-diacetyl-2′,3‴-diethylbiferrocene (0.2 g, 14%). The last band eluting with hexane/ethyl acetate (5:1) was 1′,1‴-diacetyl-3′,3‴-diethylbiferrocene (0.10 g, 7%). The physical properties of **26** are as follows. $^1$H NMR ($CDCl_3$, ppm) 1.06 (m, 6H, $-CH_3$), 2.12 (s, 3H, $-COCH_3$), 2.16 (s, 3H, $-COCH_3$), 2.18 (q, 2H, $-CH_2-$), 2.39 (m, 1H, $-CH-$), 2.62 (m, 1H, $-CH-$), 4.16 (t, 1H, Cp), 4.20 (s, 6H, Cp), 4.26 (s, 4H, Cp), 4.39 (s, 1H, Cp), 4.45 (s, 1H, Cp), 4.90 (s, 1H, Cp). Mass spectrum: $M^+$ at *m*/*z* 510. The physical properties of 1′,1‴-diacetyl-3′,3‴-diethyl-biferrocene are as follows. $^1$H NMR ($CDCl_3$, ppm): 1.08 (t, 6H, $-CH_3$), 2.12 (s, 6H, $-COCH_3$), 2.18 (q, 4H, $-CH_2-$), 4.20 (m, 6H, Cp), 4.28 (m, 4H, Cp), 4.45 (s, 2H, Cp), 4.49 (m, 2H, Cp). Mp: 126−128 °C. Mass spectrum: $M^+$ at *m*/*z* 510.

**Reduction of 20.** The reduction reaction was carried out by carefully adding, with stirring, small portions of $AlCl_3$ (0.33 g, 2.48 mmol) to a solution of **20** (0.3945 g, 0.82 mmol) in dry ether (100 mL) at 0 °C, followed by $LiAlH_4$ (0.0621 g, 1.64 mmol). After 1 h, the solution became yellow, an excess of $H_2O$ was added, and the ether layer was separated from the mixture. The ether layer was washed with saturated aqueous $NaHCO_3$ and with $H_2O$, and then it was dried over $MgSO_4$. After evaporation of the solvent, the crude product was chromatographed on $Al_2O_3$, eluting with hexane. The first band was the desired compound. The yield was approximately 90%. Physical data for **21** are as follows. $^1$H NMR ($CDCl_3$, ppm): 1.03 (m, 9H, $-CH_3$), 2.12 (m, 6H, $-CH_2-$), 3.79 (s, 1H, Cp), 3.84 (s, 4H, Cp), 3.87 (s, 2H, Cp), 4.08 (s, 2H, Cp), 4.12 (s, 2H, Cp), 4.17 (s, 2H, Cp), 4.23 (s, 2H, Cp). Mass spectrum: $M^+$ at *m*/*z* 454. Mp: 45.4−46 °C.

**Reduction of 23.** Reduction of **23** with $LiAlH_4/AlCl_3$ in ether was carried out with a procedure similar to the reduction of **20**. Data for **24** are as follows. $^1$H NMR ($CDCl_3$, ppm): 1.04 (t, 9H, $-CH_3$), 2.13 (m, 6H, $-CH_2-$), 3.74 (s, 3H, Cp), 3.83 (s, 2H, Cp), 3.85 (s, 2H, Cp), 4.06 (s, 2H, Cp), 4.11 (s, 2H, Cp), 4.16 (s, 2H, Cp), 4.24 (s, 2H, Cp). Mass spectrum: $M^+$ at *m*/*z* 454.

**Reduction of 26.** Reduction of **26** with $LiAlH_4/AlCl_3$ in ether was carried out with a procedure similar to the reduction of **20** and **23**. Data for **27** are as follows. $^1$H NMR ($CDCl_3$, ppm): 1.02 (m, 12H, $-CH_3$), 2.10 (m, 8H, $-CH_2-$), 3.79 (s, 4H, Cp), 3.86 (s, 2H, Cp), 4.10 (s, 4H, Cp), 4.18 (s, 4H, Cp). Mass spectrum: $M^+$ at *m*/*z* 482.

**Mixed-Valence Compounds 15−17.** Crystalline samples of these mixed-valence compounds were prepared by adding a benzene/hexane (1:1) solution containing a stoichiometric amount of iodine to a benzene/hexane (1:1) solution of the corresponding neutral biferrocene at 0 °C. The resulting dark green crystals were filtered off and washed repeatedly with cold hexane. Compounds were recrystallized from $CH_2Cl_2$/hexane. Anal. Calcd for **15** ($C_{26}H_{30}Fe_2I_3$): C, 37.18; H, 3.60. Found: C, 36.78; H, 3.58. Calcd for **16** ($C_{26}H_{30}Fe_2I_3$): C, 37.18; H, 3.60. Found: C, 36.52; H, 3.59. Calcd for **17** ($C_{28}H_{34}Fe_2I_3$): C, 38.97; H, 3.97. Found: C, 38.59; H, 3.90.

**Physical Methods.** $^{57}$Fe Mössbauer measurements were made on a constant-velocity instrument which was previously described. Computer fittings of the $^{57}$Fe Mössbauer data to Lorentzian lines were carried out with a modified version of a previously reported program.[15] Velocity calibrations were made using 99.99% pure 10-$\mu$m iron foil. Typical line widths for all three pairs of iron lines fell in the range 0.24−0.27 mm s$^{-1}$. Isomer shifts are reported relative to iron foil at 300 K but are uncorreted for temperature-dependent, second-order Doppler effects. It should be noted that the isomer shifts shown in the figures are plotted as experimentally obtained. Tabulated data are provided.

$^1$H NMR spectra were run on a Varian Gemini-200 spectrometer. Mass spectra were obtained with a VG-BLOTECH-QUATTRO-520 system.

Electrochemical measurements were made with a BAS 100W system. Cyclic voltammetry was performed with a stationary glassy carbon working electrode, which was cleaned after each run. These experiments were carried out with $1 \times 10^{-3}$ M solutions of biferrocene in dry $CH_2Cl_2/CH_3CN$ (1:1) containing 0.1 M $(n\text{-}C_4H_9)_4NPF_6$ as the supporting electrolyte. The potentials quoted in this work are relative to a Ag/AgCl electrode at 25 °C. Under these conditions, ferrocene shows a reversible one-electron oxidation wave ($E_{1/2} = 0.38$ V).

The near-IR spectra were recorded from 2600 to 900 nm in $CH_2Cl_2$ by using 1.0-cm quartz cells with a Hitachi U-3501 spectrophotometer.

**Crystal Structure Determinations.** Data were collected for crystals of **15** and **21** on an Enraf-Nonius CAD4 diffractometer at 298 K. Absorption corrections based on $\psi$ scans were applied. The structures were solved by the heavy-atom method. Positional and anisotropic thermal parameters for non-hydrogen atoms were refined by the full-matrix least-squares method, and H atoms were introduced in calculated positions and refined isotropically. Further details are given in Table 1. Selected bond lengths and angles are listed in Table 2. Atomic positional parameters for **15** and **21**, complete tables of interatomic distances and angles, and thermal parameters for these compounds are supplied as Supporting Information.

**1′,2′,1‴-Triethylbiferrocenium Triiodide (15).** A dark crystal measuring 0.12 × 0.16 × 0.25 mm, grown by layering hexane on a $CH_2Cl_2$ solution of **15**, was attached to a quartz fiber with hydrocarbon grease. Cell dimensions were obtained from 25 reflections with 19.72° < 2$\theta$ < 26.60°. The $\theta$-2$\theta$ scan technique was used to record the intensities for all reflections. Of these, there were 2532 reflections with $F_o > 2.0\sigma(F_o^2)$, where $\sigma(F_o^2)$ values were estimated from counting statistics. These data were used in the final refinement of structural parameters.

**Table 1.** Experimental and Crystal Data for the X-ray Structures

| | **15** | **21** |
|---|---|---|
| formula | $C_{26}H_{30}Fe_2I_3$ | $C_{26}H_{30}Fe_2$ |
| MW | 834.92 | 454.21 |
| cryst syst | monoclinic | triclinic |
| space group | $P2_1/n$ | $P\bar{1}$ |
| *a*, Å | 9.962(3) | 7.465(3) |
| *b*, Å | 20.610(3) | 8.419(2) |
| *c*, Å | 13.326(3) | 18.581(4) |
| α, deg | | 87.83(2) |
| $\beta$, deg | 92.74(2) | 87.98(3) |
| $\gamma$, deg | | 64.27(2) |
| *V*, Å$^3$ | 2732.8(1) | 1051.0(5) |
| *Z* | 4 | 2 |
| $D_{calcd}$, g cm$^{-3}$ | 2.029 | 1.435 |
| $\mu$, mm$^{-1}$ | 4.45 | 1.37 |
| $\lambda$, Å | 0.710 69 | 0.710 69 |
| 2$\theta$ limits, deg | 44.9 | 45.0 |
| transm coeff: max, min | 0.999, 0.739 | 0.998, 0.921 |
| $R_F$[a] | 0.033 | 0.021 |
| $R_{wF}$[b] | 0.036 | 0.029 |

[a] $R_F = \sum(F_o - F_c)/\sum F_o$. [b] $R_{wF} = [\sum(w(F_o - F_c)^2)/\sum(wF_o^2)]^{1/2}$.

**Table 2.** Selected Bond Lengths (Å) and Angle (deg)

| | **15** | **21** | | **15** | **21** |
|---|---|---|---|---|---|
| I1−I2 | 2.863(1) | | C1−C2 | 1.46(1) | 1.425(3) |
| I1−I3 | 2.975(1) | | C1−C5 | 1.43(1) | 1.419(3) |
| Fe1−C1 | 2.052(8) | 2.056(2) | C2−C3 | 1.42(1) | 1.425(4) |
| Fe1−C2 | 2.04(2) | 2.042(2) | C3−C4 | 1.42(1) | 1.403(4) |
| Fe1−C3 | 2.045(9) | 2.046(2) | C4−C5 | 1.41(1) | 1.417(4) |
| Fe1−C4 | 2.054(9) | 2.044(2) | C6−C7 | 1.42(1) | 1.431(3) |
| Fe1−C5 | 2.057(9) | 2.038(2) | C6−C10 | 1.45(1) | 1.428(3) |
| Fe1−C6 | 2.077(9) | 2.055(2) | C7−C8 | 1.42(2) | 1.416(4) |
| Fe1−C7 | 2.058(8) | 2.054(2) | C8−C9 | 1.44(2) | 1.413(4) |
| Fe1−C8 | 2.04(1) | 2.039(3) | C9−C10 | 1.42(1) | 1.401(4) |
| Fe1−C9 | 2.048(9) | 2.031(3) | C11−C12 | 1.42(1) | 1.427(3) |
| Fe1−C10 | 2.063(9) | 2.04(2) | C11−C15 | 1.43(1) | 1.425(3) |
| Fe2−C11 | 2.144(8) | 2.058(2) | C12−C13 | 1.43(1) | 1.423(3) |
| Fe2−C12 | 2.091(9) | 2.0401(2) | C13−C14 | 1.41(2) | 1.405(4) |
| Fe2−C13 | 2.05(1) | 2.040(2) | C14−C15 | 1.43(1) | 1.422(4) |
| Fe2−C14 | 2.074(9) | 2.051(2) | C16−C17 | 1.42(1) | 1.415(4) |
| Fe2−C15 | 2.098(9) | 2.042(2) | C16−C20 | 1.42(1) | 1.411(4) |
| Fe2−C16 | 2.133(9) | 2.053(2) | C17−C18 | 1.44(1) | 1.414(4) |
| Fe2−C17 | 2.130(9) | 2.041(2) | C18−C19 | 1.41(2) | 1.399(4) |
| Fe2−C18 | 2.066(9) | 2.044(3) | C19−C20 | 1.41(2) | 1.417(4) |
| Fe2−C19 | 2.05(1) | 2.042(2) | I(2)−I(1)−I(3) | 178.64(3) | |
| Fe2−C20 | 2.07(1) | 2.044(2) | | | |

**1′,2′,1‴-Triethylbiferrocene (21).** An orange crystal measuring 0.42 × 0.35 × 0.45 mm, grown by slow evaporation from a hexane solution, was used for data collection. Cell dimensions were obtained from 25 reflections with 16.24° < 2$\theta$ < 30.42°. Data were collected to a 2$\theta$ value of 45.0°. Of the 2724 unique reflections, there were 2421 reflections with $F_o > 2.0\ \sigma(F_o^2)$.

## Results and Discussion

**Structural Studies.** X-ray crystallographic studies were undertaken to help elucidate the structures and the assignment of oxidation state for a given ferrocenyl moiety. Figures 1 and 2 display the ORTEP drawing of the neutral compound **21** and the mixed-valence compound **15**. They adopt the usual trans conformation as found for most biferrocenes and biferrocenium cations.[3] Only a few cis-conformation biferrocenes are known, and in all cases, the molecule is held in a cis conformation by a bridge between the 2 and 2″ positions of the fulvalenide

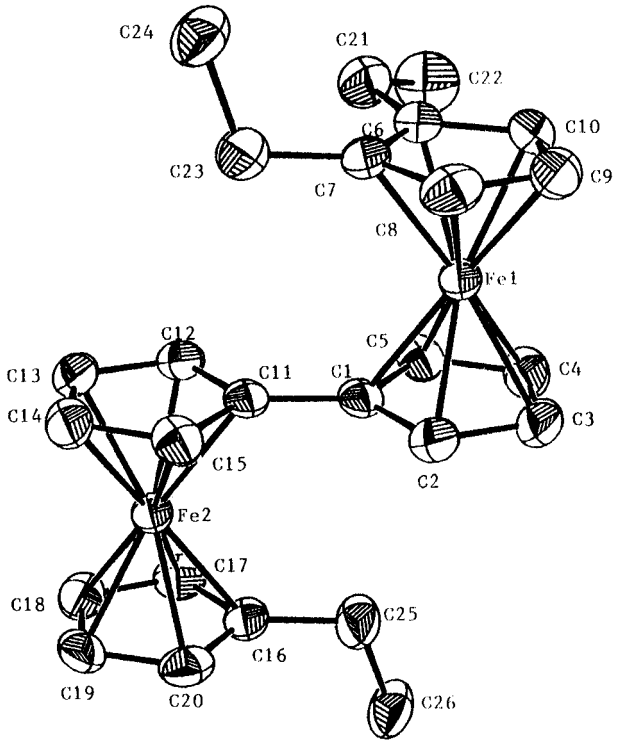


**Figure 1.** ORTEP drawing of mixed-valence compound **21**.

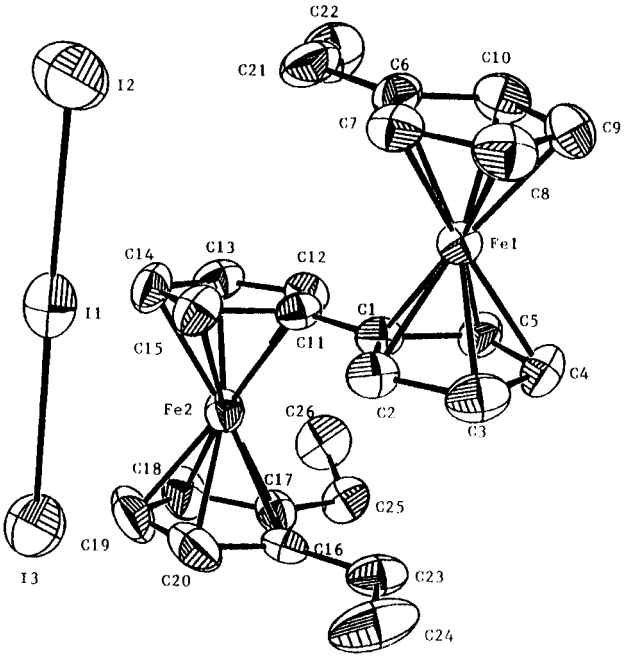


**Figure 2.** ORTEP drawing of **15**.

ligand.[21] In some cases, there are bulky substituents at the 2 and 2″ positions of the fulvalenide ligand, and the two metallocene units are twisted relative to each other.[7] The dihedral angle between the two Cp rings in the fulvalenide ligand could be as large as 42°. The dihedral angles between the two Cp rings in the fulvalenide ligands in **15** and **21** are nearly planar at 8.2(4) and with 0.8(1)°, respectively. Compounds **21** and **15** crystallize as triclinic in space group $P\bar{1}$ and as monoclinic in space group $P2_1/n$, respectively. In **15**, the dihedral angles between the two least-squares planes of the Cp rings respectively associated with Fe1 and Fe2 are 3.8(4) and 4.7(4)°, while the average staggering angles for the two Cp rings in each ferrocenyl moiety are 1.3(6) and 12.2(6)°. The two Cp rings associated with Fe1 and Fe2 in **21** are nearly eclipsed with average staggering angles of 5.3(2) and 3.1(2)°. Furthermore, the two Cp rings bonded to Fe1 and Fe2 form dihedral angles of 0.4(1) and 0.4(1)° with the fulvalenide plane, respectively. The average C−C bond lengths in the Cp rings of **15** (1.42(1) Å) and **21** (1.417(4) Å) agree well with those in ferrocene (1.42 Å)[22] and ferrocenium cations (∼1.42 Å).[23]

Inspection of the iron to Cp ligand bond lengths (1.650(1) Å associated with Fe1 and 1.653(1) Å associated with Fe2) in **21** shows that the average distance is very similar to the value of 1.65 Å found for ferrocene.[22] The average Fe−C bond distance of 2.045(2) Å also agrees well with that in ferrocene (2.045 Å).[22] These comparisons indicate that both Fe1 and Fe2 are in the Fe(II) oxidation state. In the case of **15**, the two metallocene moieties in the cation are also not equivalent. In comparison with those of ferrocene and **21**, the average Fe1−C distance (2.050(9) Å) and the average Fe1−Cp distance (1.656(4) Å) indicate that this metallocene ($Fe1(Cp)_2$) is in the Fe(II) oxidation state. The average Fe2−Cp distance (1.704(5) Å) and the average Fe2−C distance (2.091(9) Å) indicate that this metallocene ($Fe2(Cp)_2$) is in the Fe(III) oxidation state. Such an increase in Fe−C and Fe−Cp distances has been observed when ferrocene is oxidized to the corresponding ferrocenium cation.[15] Furthermore, the two-electron-donating ethyl substituents on the $Fe2(Cp)_2$ moiety stabilize the ferrocenium cation, lowering the oxidation half-wave potential. The observation of two Fe(II) and Fe(III) moieties is also consistent with our Mössbauer studies.

The triiodide anion in **15** is essentially linear. The I2−I1−I3 angle is 178.64(3)° and is comparable to the corresponding values of 177.90(4) and 177.17(5)° observed in the triiodide salt of *exo,exo*-1,12-dimethyl[1,1]ferrocenophanium[24] and diferrocenylselenium.[25] There is asymmetry associated with the bond lengths in the triiodide anion. The I1−I2 distance is 2.863(1) Å, while the I1−I3 distance is 2.975(1) Å. In other words, the triiodide anion has $I-I\cdots I^-$ characteristic. The stereopacking arrangement of **15** is shown in Figure 3. As shown in Figure 3, ion pairs exist in the solid state structure with the $I_3^-$ anion more closely associating with the Fe2(III) half of the mixed-valence cation. Thus, the $I_3^-$ anion is asymmetrically disposed relative to the two iron ions in the cation. One of the negative-charge-carrying terminal atoms (I3) is close to Fe2. This asymmetric placement of the $I_3^-$ anion relative to the cation should influence the rate of electron transfer in the cation.[26] In the solid state, the relatively minor perturbations caused by interactions between neighboring cations and anions have pronounced effects on the ET rate. When the $I_3^-$ counterion is thermally activated, it interconverts between two configurations, $I_a^-\cdots I_b-I_c$ and $I_a-I_b\cdots I_c^-$. The oscillatory charge motion associated with it controls whether charge can be pulled back and forth in the mixed-valence cation.

In **15**, a three-dimensional hydrogen bonding is clearly found between the Cp hydrogen atoms and the iodine atoms (∼3.5 to ∼4.0 Å). There is also a hydrogen bond network between the ethyl groups and triiodide anions. As shown in Figure 4, the packing arrangement of the cation cannot be described as the

(21) Zhang, W.; Wilson, S. R.; Hendrickson, D. N. *Inorg. Chem.* **1989**, *28*, 4160 and references therein.

(22) Seiler, P.; Dunitz, J. D. *Acta Crystallogr., Sect. B* **1979**, *35*, 1068.
(23) Mammano, N. J.; Zalkin, A.; Landers, A.; Rheingold, A. L. *Inorg. Chem.* **1977**, *16*, 297.
(24) Moore, M. F.; Wilson, S. R.; Cohn, M. J.; Dong, T.-Y.; Mueller-Westerhoff, U. T.; Hendrickson, D. N. *Inorg. Chem.* **1985**, *24*, 4559.
(25) Kramer, J. A.; Herbstein, F. H.; Hendrickson, D. N. *J. Am. Chem. Soc.* **1980**, *102*, 2293.
(26) Michiko, K.; Sano, H.; Iijima, S. *Bull. Chem. Soc. Jpn.* **1982**, *55*, 2327.

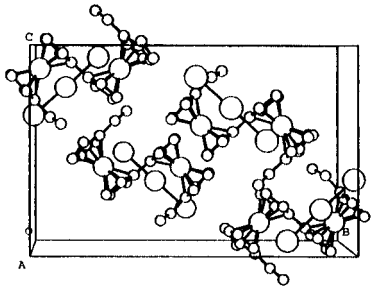

**Figure 3.** Stereopacking arrangement of **15**.

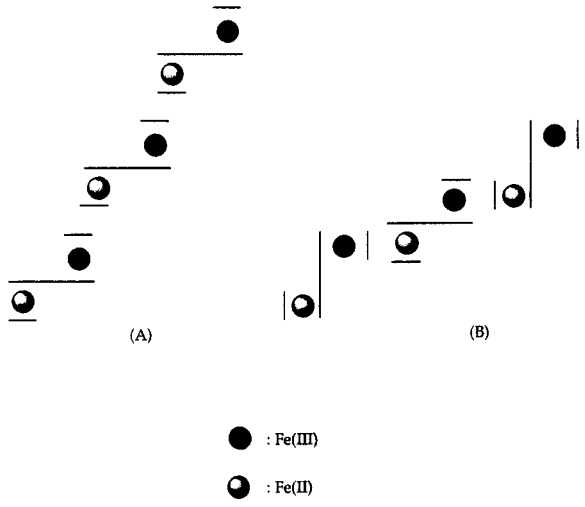


**Figure 4.** Stacking models for (A) **1**−**3** and (B) **15**.

**Table 3.** Electrochemical Data for Various Ferrocenes and Biferrocenes

| compound | $E_{1/2}$,[a] v | $E_{1/2}$,[b] v | Δ,[c] mV | $I_c/I_a$[d] |
|---|---|---|---|---|
| ferrocene | 0.38 | | 70 | 1.01 |
| 1-ethylferrocene | 0.33 | | 65 | 1.15 |
| 1,2-diethylferrocene | 0.28 | | 75 | 1.14 |
| 1,3-diethylferrocene | 0.29 | | 64 | 1.14 |
| 1′,2′,1‴,2‴-tetraethylbiferrocene | 0.16 | 0.37 | 71 | 0.88 |
| | 0.53 | | 71 | 1.00 |
| 1′,3′,1‴,3‴-tetraethylbiferrocene | 0.15 | 0.37 | 67 | 1.03 |
| | 0.52 | | 65 | 0.98 |
| **21** | 0.18 | 0.38 | 64 | 1.04 |
| | 0.56 | | 62 | 1.01 |
| **24** | 0.18 | 0.38 | 69 | 1.09 |
| | 0.56 | | 65 | 0.95 |
| **27** | 0.16 | 0.37 | 70 | 1.08 |
| | 0.53 | | 67 | 0.87 |

[a] All half-wave potentials are referred to the Ag/AgCl electrode. [b] Peak separation between two waves. [c] Peak-to-peak separation between the resolved reduction and oxidation wave maxima. [d] Peak current ratio between cathode and anode.

steplike columns found in the series of mixed-valence biferrocenium salts **1**−**4**. In **15**, there is no Cp−Cp overlap between neighboring cations in the solid-state structure. In the case of **3**, the Cp−Cp interplanar distance was ∼3.5 Å and an intermolecular $\pi-\pi$ interaction was expected between neighboring cations.

**Electrochemical Results.** Electrochemical data for the neutral compounds (**21**, **24**, and **27**), as well as those for some other relevant compounds, are shown in Table 3. These binuclear biferrocenes all undergo two successive reversible one-electron oxidations to yield the mono- and then the dication. Electrochemical reversibility was demonstrated by the peak-to-peak separation between the resolved reduction and oxidation wave maxima (Δ in Table 3) and a 1:1 relationship of the cathodic and anodic peak currents ($I_c/I_a$ in Table 3).

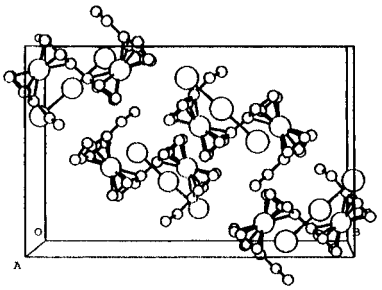

**Table 4.** Absorption Maxima of IT Bands

| compd | $\nu_{max}$[a] | $\epsilon_{max}$[b] | $\Delta\nu_{1/2(obsd)}$[c] |
|---|---|---|---|
| **15** | 4805 | 1157 | 3394 |
| **16** | 4776 | 1218 | 3342 |
| **17** | 4458 | 1305 | 3438 |

[a] In $cm^{-1}$. [b] In $M^{-1}$ $cm^{-1}$. [c] Bandwidth (in $cm^{-1}$) at half-maximum.

The effect of ethyl substituents on the stability of the Fe(III) state is illustrated by the shift of half-wave potentials. In a general way, electron-donating groups stabilize the ferrocenium cation, lowering the half-wave potential, while electron-withdrawing groups have the opposite effect. The comparison of the half-wave potentials of **21**, **24**, and **27** with those of biferrocene and 1′,1‴-diethylbiferrocene indicates that the ethyl substituent clearly acts as a net electron donor. For example, the first half-wave potential (0.18 V) of **21** is less than that (0.20 V) of 1′,1‴-diethylbiferrocene. From the electron-donating effect of the ethyl substituent, we believe that the first oxidation in **21** and **24** occurs at the Fe2 ferrocenyl moiety (eq 1).

$$C_2H_5\text{-Fc Fc-}(C_2H_5)_2 \underset{+e}{\overset{-e}{\rightleftharpoons}} C_2H_5\text{-Fc Fc}^+\text{-}(C_2H_5)_2 \underset{+e}{\overset{-e}{\rightleftharpoons}} C_2H_5\text{-Fc}^+ \text{Fc}^+\text{-}(C_2H_5)_2 \quad (1)$$

where Fc represents a ferrocenyl moiety

Furthermore, this is also consistent with our X-ray structural study. It the case of **27**, it is difficult to predict which ferrocenyl moiety is oxidized first from the ethyl substituent effect.

It has been demonstrated that the magnitude of the peak-to-peak separation ($\Delta E_{1/2}$) gives an indication of the interaction between two Fe sites.[27] A comparison of the magnitude of $\Delta E_{1/2}$ for various ethyl-substituted biferrocenes indicates that the magnitudes of interactions between the two Fe sites in symmetric and asymmetric biferrocenium cations are similar in the solution state. This indicates that the interaction between two Fe sites is insensitive both to the position of substitution and to the nature of the substituent. Thus, the zero-point energy difference ($E_0$) between two vibronic states for each asymmetric biferrocenium cation is rather small, which is reasonable in terms of the small effect of the ethyl substituent on the structure of the biferrocenium cation in the solution state.

**Electron Transfer in the Solution State.** As shown in Table 4, the asymmetrically substituted mixed-valence compounds **15**−**17** have intervalence transition (IT) bands at 4805, 4776, and 4458 $cm^{-1}$, respectively. These bands are not observed in

(27) (a) Atzkern, H.; Huber, B.; Köhler, F. H.; Müller, G.; Müller, R. *Organometallics* **1991**, *10*, 238. (b) Bunel, E. E.; Campos, P.; Ruz, P.; Valle, L.; Chadwick, I.; Ana, M. S.; Gonzalez, G.; Manriquez, J. M. *Organometallics* **1988**, *7*, 474. (c) Cowan, D. O.; Shu, P.; Hedberg, F. L.; Rossi, M.; Kistenmacher, T. J. *J. Am. Chem. Soc.* **1979**, *101*, 1304. (d) Moulton, R.; Weidman, T. W.; Vollhardt, K. P. C.; Bard, A. *J. Inorg. Chem.* **1986**, *25*, 1846. (e) Obendorf, D.; Schottenberger, H.; Rieker, C. *Organometallics* **1991**, *10*, 1293.

**Table 5.** $^{57}$Fe Mössbauer Least-Squares-Fitting Parameters

| compd | $T$, K | $\Delta E_Q$[a] | $\delta$[b] | $\Gamma$[c] |
|---|---|---|---|---|
| **15** | 300 | 2.178 | 0.457 | 0.248, 0.249 |
| | | 0.408 | 0.445 | 0.360, 0.384 |
| | 80 | 2.189 | 0.533 | 0.254, 0.206 |
| | | 0.419 | 0.513 | 0.342, 0.337 |
| **16** | 300 | 2.110 | 0.459 | 0.243, 0.244 |
| | | 0.466 | 0.440 | 0.423, 0.432 |
| | 80 | 2.116 | 0.525 | 0.256, 0.263 |
| | | 0.510 | 0.526 | 0.400, 0.416 |
| **17** | 300 | 1.804 | 0.459 | 0.284, 0.310 |
| | | 0.706 | 0.442 | 0.274, 0.301 |
| | 80 | 1.943 | 0.534 | 0.291, 0.296 |
| | | 0.689 | 0.519 | 0.295, 0.292 |

[a] Quadrupole splitting (in mm s$^{-1}$). [b] Isomer shift (in mm s$^{-1}$). [c] Full width at half-height taken from the least-squares-fitting program. The width for the line at more positive velocity is listed first for the doublet.

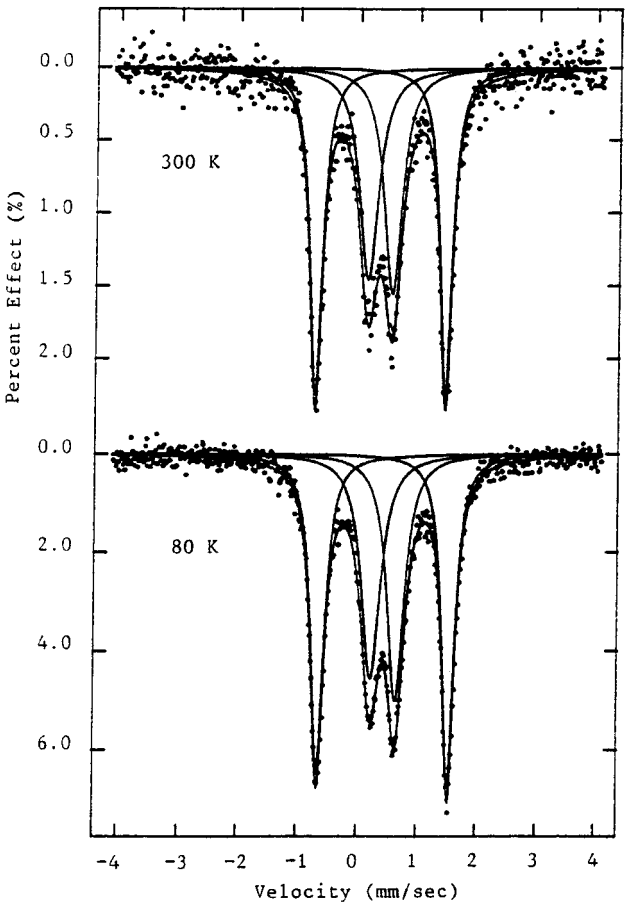


**Figure 5.** $^{57}$Fe Mössbauer spectra of **15**.

the spectra of the dications or neutral species. According to Hush's model,[20] the energy ($E_{op} = h\nu_{max}$) of an IT band is greater than or equal to 4 times the activation energy for thermal electron transfer ($E_{th}$). The energy of the band maximum ($E_{op}$) is equal to the sum of the Frank−Condon energy ($E_{FC}$) for a symmetrical one-electron transfer plus the zero-point energy difference ($E_0$) between the two vibronic states. Thus, the Hush model predicts that the IT band will be blue-shifted relative to the symmetrical case. For an unsymmetrically substituted mixed-valence compound, electron transfer will result in the formation of an energetically unfavorable valence isomer. Our results agree well with Hush's prediction. The asymmetrically substituted mixed-valence cation **15** or **16** in $CH_2Cl_2$ solution has an IT band at higher energy than the asymmetric mixed-valence cation of **17**. The observed blue shift and the magnitude of zero-point energy difference are clearly correlated.

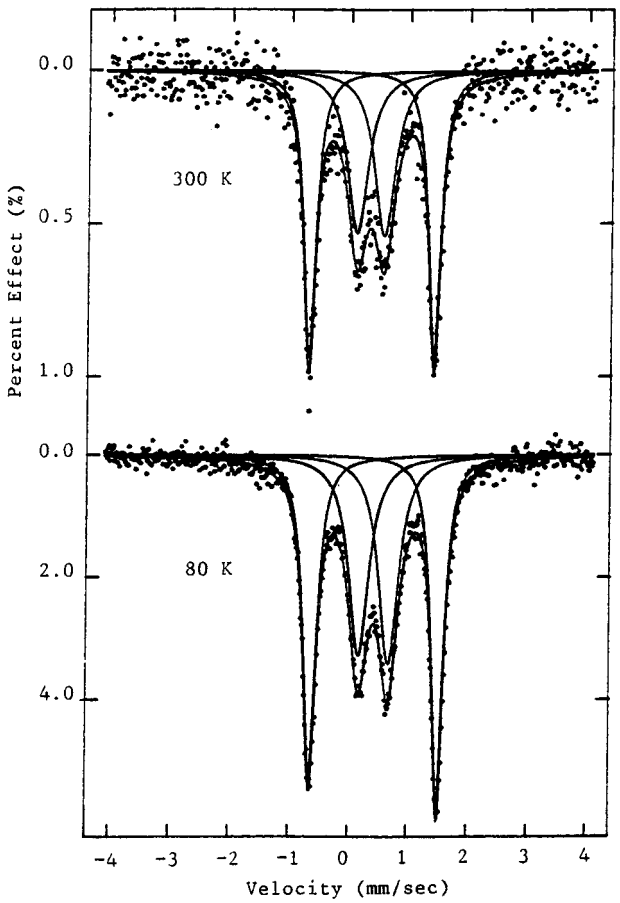


**Figure 6.** $^{57}$Fe Mössbauer spectra of **16**.

**$^{57}$Fe Mössbauer Characteristics.** Mössbauer spectra were run for **15**−**17**. The various absorption peaks in each spectrum were fitted to Lorentzian lines, and the resulting fitting parameters are summarized in Table 5. The 300 and 80 K Mössbauer spectra of these compounds are also shown in Figures 5−7. The features in all these spectra include two doublets, one with a quadrupole splitting ($\Delta E_Q$) of ~2 mm s$^{-1}$ (Fe(II) site) and the other with $\Delta E_Q$ = ~0.5 mm s$^{-1}$ (Fe(III) site). Both doublets have the same area, as deduced by a least-squares fitting. This pattern of two doublets is expected for a mixed-valence biferrocenium cation which is valence-trapped on the time scale of the Mössbauer technique (electron-transfer rate <~$10^7$ s$^{-1}$ in the solid state).

In general, the ferrocenyl group (electronic ground state $^1A_{1g}$) gives a spectrum characterized by large $\Delta E_Q$ in the range 2.0−2.2 mm s$^{-1}$, while the spectrum of the ferrocenium cation (electronic ground state $^2E_{2g}$) is characterized by small or vanishing $\Delta E_Q$.[28] In the case of localized mixed-valence biferrocenium triiodide, the value of $\Delta E_Q$ for the ferrocenyl moiety is slightly smaller than what is expected for a Fe(II) ferrocenyl moiety and the Fe(III) ferrocenium moiety has a large $\Delta E_Q$ value. This is a reflection of the admixture of Fe(II) and Fe(III) moieties into the ground state.[3,28] Therefore, the decrease of $\Delta E_Q$ in the ferrocenyl doublet and the increase of $\Delta E_Q$ in the ferrocenium doublet are an indication of the magnitude of intramolecular electron-transfer rate in the mixed-valence biferrocenium cation. At 300 K, the respective values of $\Delta\Delta E_Q$, which is the difference of $\Delta E_Q$ between Fe(II) and Fe(III) moieties, for **15**−**17** are 1.770, 1.644, and 1.098 mm s$^{-1}$. Thus, the order of the intramolecular electron-transfer rate is **17** > **16** > **15**. It is possible that the difference in rates of electron

(28) Morrison, W. H., Jr.; Hendrickson, D. N. *Inorg. Chem.* **1975**, *14*, 2331.

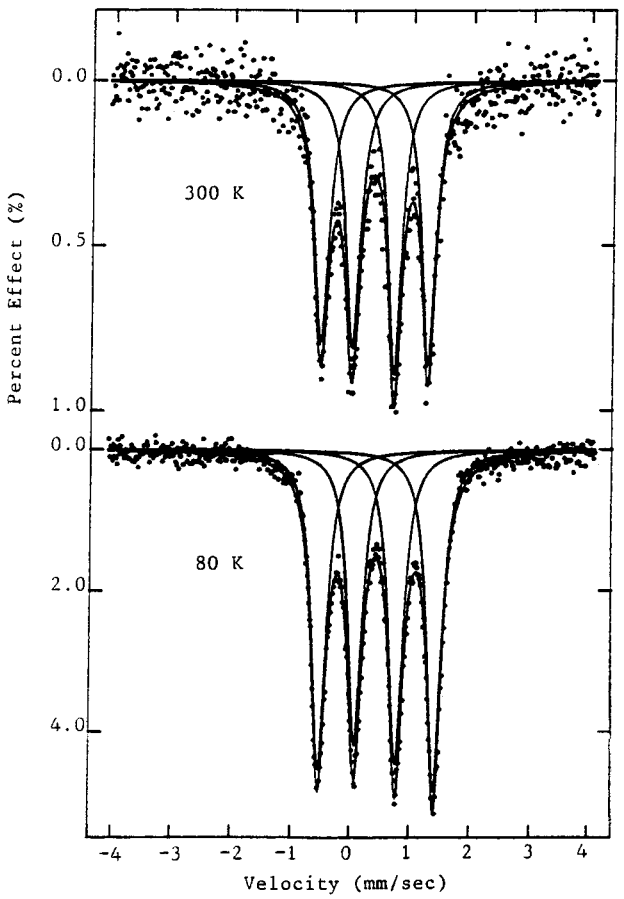


**Figure 7.** $^{57}$Fe Mössbauer spectra of **17**.

**Table 6.** $^{1}$H NMR Data for Paramagnetic Mixed-Valence Compounds in $CDCl_3$ at 298 K

| compd | exptl shift[a] $\delta$, ppm | line width, Hz |
|---|---|---|
| $(C_5H_5)_2FeI_3$ | 31.9 | 620 |
| **15** | −13.15 (2H, −CH−) | 154 |
| | −2.02 (6H, $-CH_3$) | 39 |
| | 3.15 (2H, −CH−) | 109 |
| | 3.77 (3H, $-CH_3$) | 25 |
| | 6.38 (2H, Cp) | 138 |
| | 7.77 (2H, Cp) | 110 |
| | 12.67 (2H, Cp) | 105 |
| | 14.11 (2H, $-CH_2-$) | 64 |
| | 15.05 (2H, Cp) | 133 |
| | 23.16 (3H, Cp) | 627 |
| | 27.98 (2H, Cp) | 764 |
| | 32.59 (2H, Cp) | 602 |
| **16** | −7.38 (4H, $-CH_2-$) | 157 |
| | −4.66 (6H, $-CH_3$) | 53 |
| | 3.79 (3H, $-CH_3$) | 23 |
| | 5.97 (2H, Cp) | 138 |
| | 7.83 (2H, Cp) | 103 |
| | 12.75 (2H, Cp) | 107 |
| | 14.20 (2H, $-CH_2-$) | 64 |
| | 15.11 (2H, Cp) | 107 |
| | 24.6 (2H, Cp) | 620 |
| | 28.3 (3H, Cp) | 683 |
| | 33.2 (2H, Cp) | 564 |
| **17** | −1.87 (2H, −CH−) | 104 |
| | −0.64 (6H, $-CH_3$) | 38 |
| | 1.01 (6H, $-CH_3$) | 38 |
| | 1.37 (4H, $-CH_2-$) | 177 |
| | 7.85 (2H, −CH−) | 111 |
| | 18.17[b] (∼13H, Cp) | 625 |
| | 20.58[b] (∼4H, Cp) | 303 |

[a] Shifts were taken relative to the TMS peak. [b] Overlap.

transfer in **15**−**17** is a result of the magnitude of the zero-point energy difference.

As mentioned in the Introduction, the symmetric mixed-valence compounds **9** and **12** have a delocalized electronic structure above 195 K and above 130 K, respectively.[16,17] However, the 300 K Mössbauer spectra of asymmetric mixed-valence compounds **15**−**17** indicate the presence of localized electronic structure. Hence, we suggest that the most important factor in controlling the intramolecular electron transfer in **15**−**17** is the symmetry of the cation. The cations of **15**−**17** are asymmetric; that is, the two irons are not in equivalent environments. This asymmetry results in a zero-point energy difference for intramolecular electron transfer. Thus, one vibronic state of the mixed-valence cation is energetically more stable than the other state. This explains why a localized electronic structure for **15**−**17** was observed.

**Nuclear Magnetic Resonance.** The study of nuclear resonance in paramagnetic complexes can yield detailed information concerning metal−ligand bonding and electron delocalization. It is of value to apply the NMR technique to elucidate the nature of electron delocalization in the series of mixed-valence biferrocenium salts. The $^{1}$H NMR spectra were obtained from deoxygenated $CDCl_3$ solutions. The shifts for the molecules of interest is shown in Table 6.

The two respective upfield-shifted lines at −7.38 and −4.66 ppm in the $^{1}$H NMR spectrum of **16** must be assigned to the methylene and methyl protons in the 1′,3′-diethylferrocenium moiety on the basis of intensity measurements. The corresponding peaks at 3.79 and 14.20 ppm are also assigned to the methyl and methylene protons in the 1′-ethylferrocenyl moiety on the basis of intensity measurements and line widths. The peaks at 5.97, 7.82, 12.75, and 15.11 ppm are assigned to the Cp protons in the 1′-ethylferrocenyl moiety on the basis of line widths. In comparison with the line width of Cp protons in the $^{1}$H NMR spectrum of ferrocenium triiodide, the rather broadened peaks (line width >570 Hz) at 24.6, 28.3, and 33.2 ppm must be assigned to the Cp protons in the Fe(III) 1′,3′-diethylferrocenium moiety. Thus, all Cp protons in the cation of **16** have negative spin density and positive contact shifts relative to the shifts of the corresponding neutral biferrocene. Making a comparison of the sign of contact shifts of the ethyl substituents attached to the Fe(III) 1′,3′-diethylferrocenium moiety with that of the contact shifts of the Cp protons in **16** leads to the conclusion that the unpaired electron density in this ferrocenium unit is delocalized in $\pi$ Cp orbitals, as found in ferrocenium and 1,1′-dimethylferrocenium ions.[29−31] The $\pi$-polarization effect in metallocenes was first discussed by Levy and Orgel in 1960. It was suggested that the unpaired $\pi$ electron in the Cp orbitals polarizes the C−H $\sigma$ bond. This would lead to negative spin density and positive contact shifts at the protons in metallocenes. Rettig,[29] Materikova,[30] and Kurbanov[31] reported the $^{1}$H and $^{13}$C NMR spectra of ferrocenium and 1,1′-dimethylferrocenium ions. For the 1,1′-dimethylferrocenium cation, the negative spin density at Cp protons and the positive spin density at methyl protons led the authors to propose the $\pi$-skeleton spin delocalization. However, Kurbanov found[24] that the $\sigma$ skeleton plays a more important role in the case of the decamethylferrocenium cation. In general, the mechanism of the spin delocalization of the paramagnetic ferrocenium cation depends on the superposition of the $\pi$ and $\sigma$ mechanisms. Hence, it was not surprising to observe the delocalization of

(29) Rettig, M. F.; Drago, R. S. *J. Am. Chem. Soc.* **1969**, *91*, 1361.
(30) Materikova, R. B.; Babin, V. N.; Solodovnikov, S. P.; Lyatifov, I. R.; Petrovsky, P. V.; Fedin, E. I. *Z. Naturforfsch., B: Anorg. Chem. Org. Chem.* **1980**, *35*, 1415.
(31) Kurbanov, T. *Kh. Azerb. Khim. Zh.* **1981**, *6*, 104.

unpaired electron density in $\sigma$ Cp orbitals of the Fe(II) 1‴-ethylferrocenyl moiety in cation **16**. In the $^1$H NMR spectrum of **16**, the negative spin density at Cp protons and ethyl protons in the Fe(II) 1‴-ethylferrocenyl moiety strongly suggests that the unpaired spin density is in fact in Cp $\sigma$ orbitals rather than in $\pi$ orbitals. Electron delocalization in $\sigma$ orbitals has been observed for 1,1′-dimethylchromocene,[29] nickel pyridine complexes,[32] and aliphatic amines.[33]

The shifts in the $^1$H NMR spectrum of **15** are similar to those of **16**, except for the shifts of the ethyl protons in the Fe(III) 1′,3′-diethylferrocenium moiety. The two upfield lines at −13.15 and −2.02 ppm in the spectrum of **15** are assigned to one of methylene protons and methyl protons, respectively. In comparison with the spectrum of **16**, the peak which appeared at 3.15 ppm could be assigned to another methylene proton. It is clear that the two methylene protons have different signs of spin density. The observed different sign for methylene protons suggests that the nature of electron delocalization involves a competition of $\sigma$ and $\pi$ mechanisms. The spin densities and the competitions of $\sigma$ and $\pi$ mechanisms are different from one cation to another. It is likely that the change of contact shifts reflects the degree of delocalization in the mixed-valence cations.

In the case of **17**, we found that there is a significant change in the features of the $^1$H NMR spectrum. As shown in Table 6, all Cp protons have negative spin densities and positive contact shifts. On the other hand, all ethyl protons have positive spin densities and negative contact shifts except one of the methylene protons in the 1′,2′-diethylferrocenium moiety. In comparison with the case of cations of **15** and **16**, this dramatic change in contact shifts suggests that the two ferrocenyl moieties in **17** have Fe(III) oxidation state character. Of course, this is a reflection of the rather small value of zero-point energy difference for the cation of **17**. Furthermore, we suggest from the comparison of the magnitudes of contact shifts that the 1′,2′-diethylferrocenium moiety has more Fe(III) character than the 1‴,3‴-diethyl-ferrocenium moiety.

## Conclusion

We have demonstrated that relatively minor perturbations caused by the nonzero zero-point energy difference have pronounced effects on electronic structure and rate of intramolecular electron transfer. Mössbauer spectra indicating the presence of localized electronic structure have been observed for **15**−**17**.

**Acknowledgment** is made to the National Science Council (Grant NSC84-2113-M-110-015) and National Sun Yat-sen University for financial support.

**Supporting Information Available:** Complete listings of atomic coordinates, thermal parameters, and bond distances and angles (11 pages). Ordering information is given on any current masthead page.

IC950953B

(32) Happe, J.; Ward, R. L. *J. Chem. Phys.* **1963**, *39*, 1211.
(33) Fitzgerald, R. J.; Drago, R. S. *J. Am. Chem. Soc.* **1968**, *90*, 2523.